A Model Study of the Effects of the Discrete Cellular Structure on Electrical Propagation in Cardiac Tissue

Yoram Rudy and WeiLun Quan

The effects of the discrete cellular structure on propagation of electrical excitation in cardiac muscle were studied in a one-dimensional fiber model containing a periodic intercalated disk structure. Globally, the macroscopic velocity of propagation follows the behavior associated with propagation in a continuous tissue (except for high values of disk resistance). In addition, the computed spatial extracellular potential along the fiber is a smooth biphasic waveform and does not reflect the underlying discrete cellular structure of the tissue. Other results of the simulations demonstrate the discontinuous nature of propagation and the importance of the structure in arrhythmogenesis. $\dot{V}_{max}$ displays a biphasic behavior as a function of increasing intercalated disk resistance. An initial "paradoxical" increase in $\dot{V}_{max}$ (with a simultaneous decrease in conduction velocity) is followed by a decrease that leads to decremental propagation and conduction block. The time constant of the foot of the action potential (τ_{foot}) increases monotonically with increasing intercalated disk resistance. An increase in the leakage current to extracellular space brings about a significant decrease in the action potential duration and a loss of the plateau. This major effect is accompanied by a relatively smaller decrease in conduction velocity. Collision of two activation wavefronts results in a significant (100%) increase in $\dot{V}_{max}$ and a very small (0.6%) decrease in τ_{foot}. (*Circulation Research* 1987; 61:815–823)

The anatomical structure of the myocardium as an assembly of discrete cells separated by a periodic intercalated disk structure was established in 1954. However, until recently the propagation of electrical excitation in cardiac muscle has been characterized as though it occurred in a syncytium. The effects of the structural discontinuities introduced by the disks were not considered important, and activation was analyzed on the basis of continuous models utilized successfully for nerves (one-dimensional continuous cable theory).[1] Moreover, various (normal and abnormal) characteristics of propagation were traditionally associated with membrane properties alone, while effects of the anatomical structure of the myocardium were, for the most part, ignored. Such propagation phenomena include slow conduction, decremental conduction, conduction block, and changes in action potential duration and refractory periods. All of these characteristics are recognized as conditions that play an important role in causing reentrant arrhythmias.

Recent experimental results[2,3] showed electrical properties of cardiac muscle that could not be explained on the basis of continuous cable theory. For example, $\dot{V}_{max}$ (maximum rate of change of the temporal action potential) was observed to increase as propagation velocity decreased due to a wider angle of propagation relative to the fiber axis. This result is in contrast to the direct relation between $\dot{V}_{max}$ and velocity predicted by continuous models and often used in the interpretation of results obtained in cardiac tissue. In addition, the importance of the anatomical structure of cardiac muscle in determining conduction velocity and source configuration,[4–6] as well as its possible role in causing conduction abnormalities such as slow conduction, conduction block, and reentry was recently established.[2,7–9] It is clear that the effects described above and the possibility that they arise from the discrete cellular structure of the myocardium can only be examined using a model that includes microscopic discontinuities (intercalated disks) at the cellular level. The effects of a discrete pattern of resistive barriers on propagation of the cardiac action potential were studied by Joyner.[10] In his study, the discontinuities were introduced by discretizing a continuous cable into elements Δx equal to the cell length. Both the cytoplasmic resistance and junctional resistance were incorporated in an effective longitudinal resistance R_i. Another aspect of propagation in a discontinuous model was studied by Steinhaus and Spitzer.[11] Their study concentrates on cell-to-cell interactions during activation sequence changes in Purkinje fibers. In the present study, a one-dimensional discontinuous model is utilized to study the effects of the periodic disk structure on propagation in cardiac muscle. It should be mentioned that this model is constructed of cells of realistic dimensions (100 μm long, and 16 μm in diameter). The resolution is such that spatial variations within a single cell can be examined. Moreover, the model does not "lump" together the myoplasmic resistance and the intercalated disk resistance and permits, therefore, the effects of the myoplasm and the effects of the disk on propagation to be studied separately. The study emphasizes the effects caused by systematic changes in disk resistance over a wide range

From the Department of Biomedical Engineering, Case Western Reserve University, Cleveland, Ohio.

Supported by National Institutes of Health grant HL 33343.

Address for correspondence: Yoram Rudy, Department of Biomedical Engineering, Case Western Reserve University, Cleveland, OH 44106.

Received May 25, 1986; accepted May 8, 1987.

Downloaded from http://ahajournals.org by on March 12, 2022

of values. This range covers normal anisotropic effects as observed by Spach and his coworkers, as well as the effects of abnormally high disk resistance (high degree of decoupling) observed in ischemia and infarction.[8,9,12] In addition, the intercalated disk model incorporates the ability to simulate effects of increased leakage to the extracellular space. An increase in the leakage current may occur in areas of damaged myocardium (ischemia, infarction) and may be responsible for the short duration action potentials observed under these conditions.[8,12]

Materials and Methods

The model (Figure 1) consists of a one-dimensional fiber that includes 40–100 individual cells (each 100 μm long, and 16 μm in diameter). Neighboring cells are connected by an intercalated disk structure modelled as a T-resistance network (two axial resistances representing the intercytoplasmic channels [connexons], and a radial leakage resistance to the extracellular space). A purely resistive network representation for the intercalated disk was adopted based on the evidence that the interaction between cells is passive[13] and the fact that the junctional axial resistance is constant over a wide range of voltages.[14] In addition, the purely resistive model of the disk neglects capacitive shunting. This approximation reflects the short time constant associated with the nexus membranes.[15,16] Each cell was discretized into three Beeler and Reuter[17] membrane patches. This division of the cell was tested for convergence. It permits the study of spatial variations within a single cell and allows us to separately study effects of the myoplasm and of the intercalated disk resistance. By combining the Beeler and Reuter membrane model with the core conductor model[18] and the periodic intercalated disk structure, we were able to develop equations for the propagating action potential V_m (x,t) at every membrane patch. The method of Cooley and Dodge[19] and the simplifying algorithm of Rush and Larsen[20] were used to compute V_m (x,t) numerically.

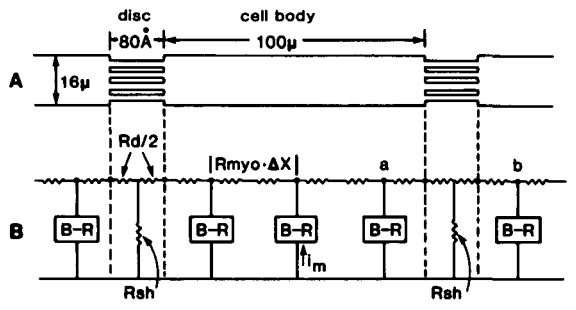

FIGURE 1. Panel A: *Discrete cable model of cylindrical cardiac cells, each 100 μm in length and 16 μm in diameter, interconnected by an intercalated disk structure that contains intercellular bridges (connexons).* Panel B: *Core conductor network with 3 Beeler and Reuter (B-R) membrane patches per cell, and a T network representing the intercalated disk between cells. R_d, disk resistance; R_{myo}, myoplasm resistivity; and R_{sh}, leakage resistance to extracellular space.*

The equation governing the behavior of $V_m(x,t)$ is the following:

$$\frac{\partial^2 V_m(x,t)}{\partial x^2} = (2/a)(R_i + R_e)\left(C_m \frac{\partial V_m(x,t)}{\partial t} + I_{ion}\right) \quad (1)$$

where I_{ion} is the membrane ionic current density, a is the radius of the fiber, C_m is the membrane capacity, and R_i and R_e are the internal and the external resistivities, respectively. I_{ion} includes four individual components of ionic current.[17] These are I_{Na}, the excitatory inward sodium current; I_s, the slow inward current, primarily carried by calcium ions; I_{K1}, the time-independent outward potassium current, and I_{X1}, the voltage- and time-dependent outward current, primarily carried by potassium ions. This term contains the stimulus current as well. For a symmetrical finite length fiber, the boundary condition at the stimulating electrode ($x=0$) is $V_{-j}=V_j$ (symmetry with respect to $x=0$). For the boundary condition at the end of the fiber, we assume $\partial V_m/\partial x=0$, implying a sealed end. All of the physiologic parameters were measured at the middle portion of the fiber, which is free of end effects and stimulus artifacts.

It should be noted that the discretization of the second spatial derivative $\partial^2 V_m(x,t)/\partial x^2$ using the second order central difference formula

$$\frac{V^K_{j+1} - 2V^K_j + V^K_{j-1}}{(\Delta X)^2} \quad (2)$$

is not valid at junctional points such as a and b in Figure 1B. This results from the asymmetry of the two resistance "arms" at these points (see figure). The use of the balanced second central difference (2) violates Ohm's law at these junctions and tends to exaggerate the discontinuous effects of the intercalated disks.[21] A modified version of equation 2, which takes into account the asymmetry in the resistances and is in accordance with Ohm's law, is shown below (2a and 2b) and was used here for computing second derivatives at the intercalated disks.

For point a (Figure 1):

$$\frac{2V^K_{j+1} - 3V^K_j + V^K_{j-1}}{(\Delta X)^2} \quad (2a)$$

For point b (Figure 1):

$$\frac{2V^K_{j-1} - 3V^K_j + V^K_{j+1}}{(\Delta X)^2} \quad (2b)$$

In addition to the transmembrane potential, the extracellular potential was also computed in this paper. The extracellular potential field of a uniform cylindrical fiber (of a cross section A) in a conducting medium of conductivity σ_e can be computed from the transmembrane potential V_m using the following integral expression[22]:

$$\phi = -\frac{\sigma_i}{4\pi\sigma_e}\int dA \int \frac{\partial V_m}{\partial X}\,\hat{a}_x \cdot \nabla\left(\frac{1}{r}\right) dx \quad (3)$$

Downloaded from http://ahajournals.org by on March 12, 2022

where σ_i is the intracellular conductivity, $\hat{a}_x$ is a unit vector in the direction of the fiber axis, and r is the distance from a source point to a field point. The above expression demonstrates that the active fiber equivalent sources can be represented by a distribution of axial dipoles that fill the intracellular space. The dipole density is uniform over a cross section but varies as $-\partial V_m/\partial x$ (the negative of the slope of the action potential) in the axial direction. This implies that the source density is very large at the disk since sharp discontinuities are introduced in the rising phase of the action potential at each intercalated disk location (see Figure 14). However, in the discontinuous model the cross section of the fiber is nonuniform (only a small fraction of the cell cross section is occupied by connexons at the cell junction and is available for axial current flow). As a result, the integral (equation 3) has to be divided into two separate contributions from the cell and from the junction with a different cross section for each.[23] A modified form of equation 3 that takes these different effective cross sections into account was utilized here for computing the extracellular potential field and is shown below (equation 3a). For a single cell that includes the cell body (myoplasm region) and an intercalated disk (junctional region), the extracellular potential field is given by

$$\phi = -\frac{\sigma_i}{4\pi\sigma_e}\left[\int dA_m \int_m \frac{\partial V_m}{\partial X}\,\hat{a}_x \cdot \nabla\left(\frac{1}{r}\right) dx + \int dA_j \int_j \frac{\partial V_m}{\partial X}\,\hat{a}_x \cdot \nabla\left(\frac{1}{r}\right) dx\right] \quad (3a)$$

where m is the axial extent of the myoplasm, and j is the axial extent of the junction. Note the separate contributions from the cell (myoplasm) and from the gap junction. Typically, the cross-sectional area of the junctional region (A_j) is only 0.03% of the cell body cross-sectional area (A_m). A summation of equation 3a over all cells and junctions in the fiber provides the total extracellular potential.

It should be mentioned here that in equation 3 an equivalent axial dipolar source density $-\partial Vm/\partial X$ is used to compute the extracellular potential. Using the one-dimensional "cable equations" it can be shown[22] that equation 3 is equivalent to the following expression:

$$\phi = \frac{1}{4\pi}\,\frac{\sigma_i}{\sigma_e}\int dA \int \frac{r_i\, i_m}{r}\, dx \quad (3b)$$

in which the source term is the transmembrane current per unit length (i_m), and r_i is the intracellular axial resistance per unit length of the fiber. While i_m is closely related to the actual biophysical sources (ionic currents in the membrane), $-\partial Vm/\partial X$ is an equivalent representation that permits an accurate and convenient computation of the extracellular potential distribution. It is particularly suitable for the discontinuous model in view of the nonuniform cross section of the fiber. As mentioned above, $-\partial Vm/\partial X$ and i_m are related by the "cable equations" and result in the same extracellular field.

Results

1. Effects of Variations in the Intercalated Disk Resistance

Under normal physiologic conditions the contributions from the myocardial cell myoplasm and from the intercalated disk to the total effective axial resistance are roughly equal. However, while the myoplasm occupies a length of 100 μm per cell in the direction of propagation, the gap junction between cells is only 80 Å in length, introducing a recurrent periodic discontinuity in the axial resistance. Moreover, the junctional resistance can be modulated and obtain very high values in abnormal cases such as ischemia and infarction leading to very slow conduction and, in the extreme case, to complete decoupling of neighboring cells and a resulting conduction block. It is clear, therefore, that the discrete recurrent junctional resistances must play an important role in the activation process in cardiac tissue. This section deals with the effects on propagation caused by changes in junctional resistance. In the simulations below, the myoplasm resistance was kept constant at the typical value of 200 Ω·cm, while the disk resistance was varied over a wide range of values (see figures). The following equation relates the various resistance parameters and is used to define the effective longitudinal resistivity:

$$R = R_{myo} + \frac{R_d}{L}$$

where R_d is the specific disk resistance (Ω·cm^2), R_{myo} represents myoplasmic resistivity (Ω·cm^2), R is the (effective) longitudinal resistivity (Ω·cm^2), and L is the cell length (distance between junctions).

1.1 Macroscopic and microscopic velocity. Two different velocities were defined: microscopic velocity ($^\theta$micro), representing the velocity of propagation inside a single cell, and macroscopic velocity ($^\theta$macro) (or average velocity, θ), representing the average velocity of propagation over many cells. Both velocities are defined in terms of the time of arrival of $\dot{V}_{max}$. The effects of variations in the effective longitudinal resistivity (brought about by changing the disk resistance for a constant myoplasm resistivity of 200 Ω·cm) on $^\theta$micro and $^\theta$macro are shown in Figure 2 (curves 1 and 2, respectively). The continuous case (no disks were included in the model) is shown for comparison in curve 3 and follows the inverse square root relation between conduction velocity and axial resistivity, as expected. As the disk resistance was varied from 0.1 Ω·cm^2 to 360 Ω·cm^2, $^\theta$micro and $^\theta$macro exhibited opposite changes. The microscopic velocity increases with increasing disk resistance, reflecting the fact that the current is more confined to the single cell and, therefore, more current is available to depolarize the

Downloaded from http://ahajournals.org by on March 12, 2022

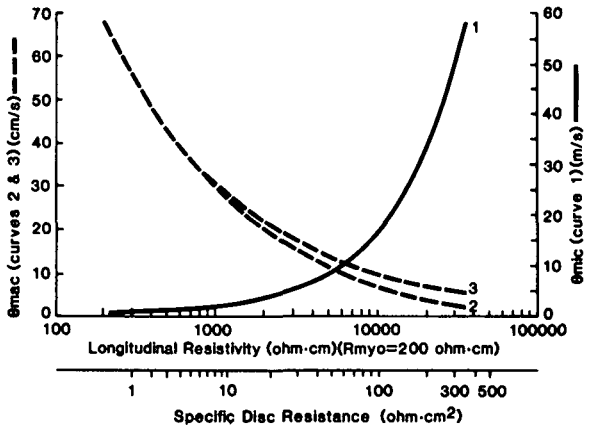

FIGURE 2. *Effects of variations in axial (longitudinal) resistivity on microscopic velocity (θmic, curve 1) and on average macroscopic velocity (θmac, curve 2). The continuous case (no disks included in the model) is shown for comparison (curve 3) and follows the inverse square root relation of continuous cable theory. The effective longitudinal resistivity is varied by varying the disk resistance while the myoplasm resistivity is kept constant at 200 Ω·cm. Both effective longitudinal resistivity and the corresponding disk resistance are indicated.*

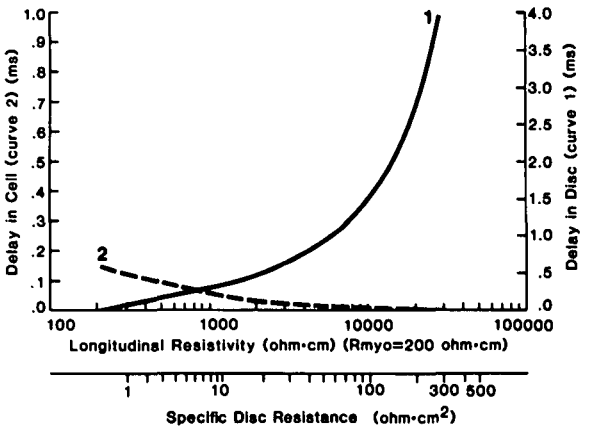

FIGURE 3. *Delay of the propagating action potential as a function of disk resistance, both in the cell (curve 2) and at the intercalated disk (curve 1).*

cellular membrane. The macroscopic (average) velocity, on the other hand, decreases with increasing disk resistance as a result of an increased time delay at the disk. In the range of effective longitudinal resistivity from 210 Ω·cm to 1,000 Ω·cm, the macroscopic velocity follows closely the inverse square root relation of continuous cable theory. However, beyond this range, changes in the disk resistance result in a greater decrease in velocity than predicted by the inverse square root relation. It will be shown below (Section 1.4) that in the range of 380 Ω·cm² to 400 Ω·cm² of disk resistance, decremental conduction is obtained in the discontinuous model, and beyond this range, complete block occurs. Note in Figure 2 the discontinuous nature of propagation with high velocity of propagation inside a cell and slower propagation over many cells. For the typical value of 2 Ω·cm² disk resistance, the microscopic velocity is twice the macroscopic velocity. This ratio increases and the discontinuous nature of propagation becomes more pronounced with increasing disk resistance (Figure 2).

The important role played by the intercalated disks in determining conduction velocity and in causing the discontinuous mode of propagation on the microscopic scale becomes apparent when the time delays of the propagating front in the cell and at the disk are examined and compared (Figure 3). For the typical values of 200 Ω·cm myoplasmic resistivity and 2 Ω·cm² disk resistance, the delay at the disk is equal to the total delay in the cell (0.1 msec). However, while the cell is 100 μm long, the gap to be traversed by the propagating action potential at the disk is only 80 Å. As the disk resistance increases (for a constant myoplasm resistance) the ratio of "disk-delay" to "cell-delay" increases quickly. For a disk resistance of 60 Ω·cm², the delay at the disk is 1.0 msec while the delay in the (much longer) cell is practically negligible. For a high disk resistance, it is clear, therefore, that the global conduction velocity is determined by the intercalated disks and that the propagation (on the microscopic scale) is highly discontinuous with the cell being depolarized as a unit (simultaneously) and a long time delay encountered by the propagating front at every disk. Globally, however, these discrete cellular effects are not apparent and the propagation appears continuous with an average uniform velocity.

1.2 $\dot{V}_{max}$ and velocity. The maximum rate of rise of the action potential $\dot{V}_{max}$ and the average macroscopic velocity (θmacro) are shown in Figure 4 (curves 1 and 2, respectively) as a function of the effective axial resistivity (again varied by increasing the disk resistance while keeping the myoplasm resistivity constant at 200 Ω·cm). The continuous case is shown for comparison in Figure 5. $\dot{V}_{max}$ displays a biphasic behavior. In the range of disk resistance from 0.1 Ω·cm² to 70 Ω·cm², $\dot{V}_{max}$ increases and conduction velocity decreases. This "paradoxical" behavior is opposite to

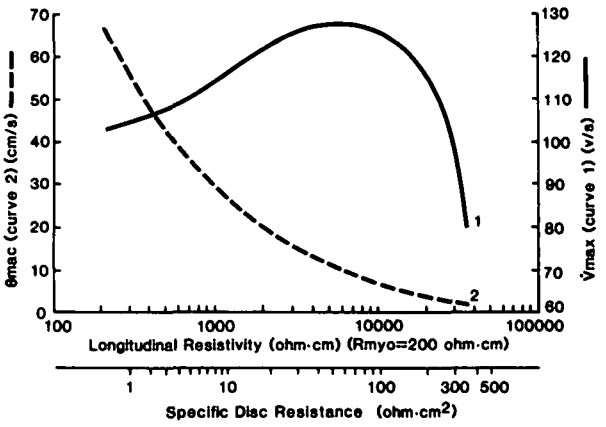

FIGURE 4. *Effects of variations in disk resistance on the macroscopic velocity of propagation (curve 2) and on the maximum rate of rise of the action potential $\dot{V}_{max}$ (curve 1).*

Downloaded from http://ahajournals.org by on March 12, 2022

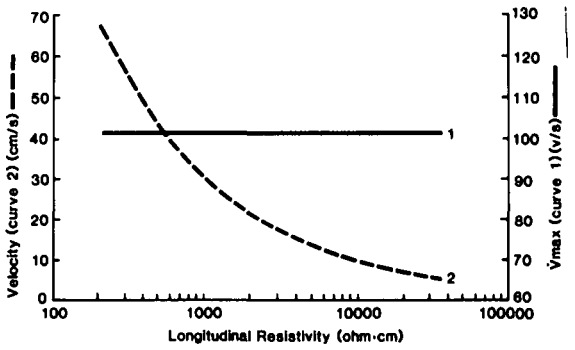

FIGURE 5. *$\dot{V}_{max}$ (curve 1) and conduction velocity (curve 2) as a function of axial resistivity for a continuous cable (no disks are included in the model).*

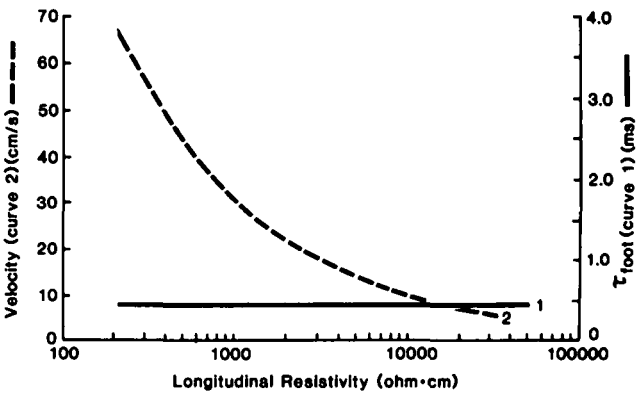

FIGURE 7. *τ_{foot} (curve 1) and conduction velocity (curve 2) as a function of axial resistivity for a continuous cable.*

the direct relation between $\dot{V}_{max}$ and conduction velocity that is predicted by continuous cable theory when the membrane sodium conductance is varied. Note that for small values of disk resistance, velocity is high and $\dot{V}_{max}$ levels off, approaching the value associated with propagation in a continuous cable (see Figure 5). For high values of disk resistance, a second phase is exhibited, and $\dot{V}_{max}$ decreases with increasing disk resistance. This part of the curve reflects the transition to decremental conduction and eventually to a complete conduction block. For a certain value of disk resistance (70 $\Omega \cdot cm^2$), $\dot{V}_{max}$ attains a maximum. For this high resistance value, the cell is separated to a large degree from its downstream neighbor, and $\dot{V}_{max}$ approaches the value that could be obtained under space-clamp condition. Note that in the continuous case (Figure 5) the velocity drops according to the inverse square root relation, and $\dot{V}_{max}$ remains constant, independent of variations in axial resistivity.

1.3 The foot of the action potential (τ_{foot}). The time constant of the "foot" of the action potential was computed (Figure 6) using the discontinuous model. The foot represents the subthreshold transmembrane potential variation preceding activation. For a uniform continuous fiber, this portion of the action potential is exponential with a time constant given by: $\tau_{foot} = 1/\theta^2 r_a c_m$ where r_a is the axial resistance and c_m is the membrane capacitance per unit length.[24] In addition, for the continuous case the velocity is proportional to the inverse square root of r_a, that is, $\theta \propto 1/\sqrt{r_a}$, and as a result $\tau_{foot} \propto 1/c_m$, independent of r_a. This relation does not apply to the actual discontinuous case. Figure 6 shows the behavior of τ_{foot} in the discontinuous model (curve 1) as a function of axial resistance (again varied by increasing the disk resistance). The macroscopic velocity is also shown (curve 2). For comparison, the continuous case is shown in Figure 7. Note that τ_{foot} increases monotonically with increasing disk resistance in the actual discontinuous case, accompanied by a decrease in velocity. As expected, no change in τ_{foot} is observed in the continuous case (Figure 7). The sensitivity of the τ_{foot} measurement to its distance from the stimulus site is simulated in Figure 8. For a stimulus of 900 $\mu A/cm^2$, τ_{foot} measured at a distance of 2 mm from the stimulus site is about 10% smaller than that at 4 mm away. This long range effect of the stimulus has to be considered in measurements of τ_{foot} from a cardiac tissue of complex geometry.

1.4 Decremental propagation. For the range of very high disk resistance (380 $\Omega \cdot cm^2$ to 400 $\Omega \cdot cm^2$)

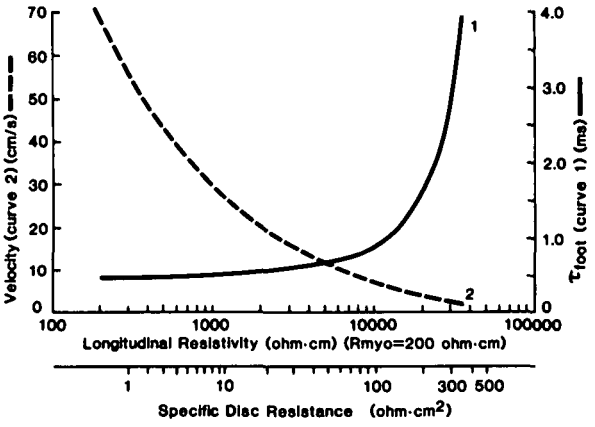

FIGURE 6. *Effects of variations in disk resistance on the macroscopic velocity (curve 2) and on the time constant of the foot of the action potential τ_{foot} (curve 1).*

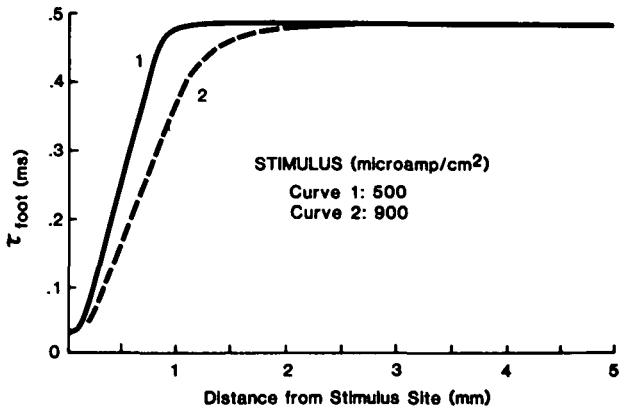

FIGURE 8. *The effect of the stimulus on τ_{foot} as a function of distance from the stimulus site. Stimuli of two different strengths are considered: 500 $\mu A/cm^2$ and 900 $\mu A/cm^2$ (curves 1 and 2, respectively).*

Downloaded from http://ahajournals.org by on March 12, 2022

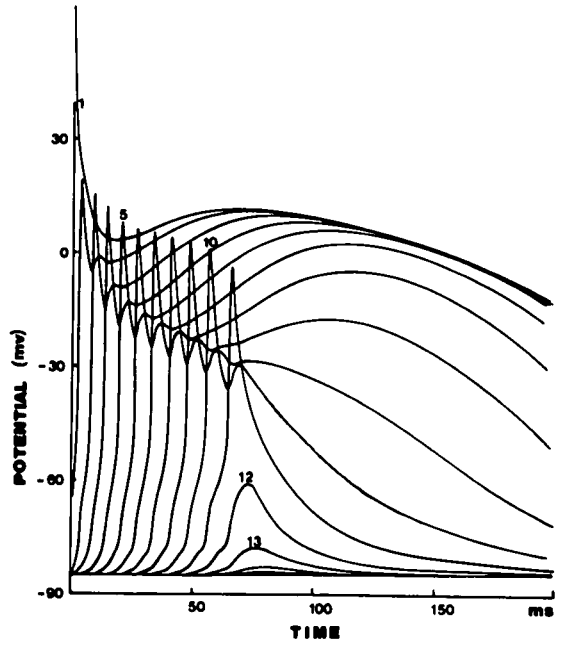

FIGURE 9. *Decremental propagation caused by a very high disk resistance (R_d, 380 Ω·cm²). Numbers in the body of figure indicate cell number relative to stimulus site.*

decremental propagation is obtained in our model simulations. This situation is shown in Figure 9. The numbers in the body of the figure indicate the cell number relative to the stimulus site. The velocity of propagation decreases progressively with distance from the stimulus site (the velocity could be as low as 1.5 cm/sec). In addition, the action potential duration and amplitude decrease. Note the spike-like appearance of the action potential, which is consistent with the experimental observations of Sasyniuk and Mendez.[25] For values of disk resistance greater than 400 Ω·cm², complete conduction block occurs.

2. *The Leakage Resistance (R_{sh})*

An increase in the leakage current to the extracellular space may occur in areas of damaged myocardium due to a decrease in the leakage resistance (R_{sh}) at the disk. The effects of such changes on the propagated action potential are simulated below. The major effect is on the action potential duration as shown in Figure 10. Curves 1 to 4 correspond to progressively decreasing values of the leakage resistance ($R_{sh} = 10^8$ kΩ, 10^7 kΩ, 10^6 kΩ, and 10^5 kΩ, respectively). As a result of the increase in leakage current, the duration of the action potential decreases progressively until the plateau is completely lost (curve 4). Note the small changes when R_{sh} is decreased from 10^8 kΩ to 10^7 kΩ. In contrast, for R_{sh} smaller than 10^7 kΩ the action potential duration decreases quickly, and this change is accompanied by a decrease in the amplitude of the plateau. A progressively increasing effect on the velocity of propagation is also observed with the values of 55.47 cm/sec, 55.40 cm/sec, 54.80 cm/sec, and 48.12 cm/sec obtained for cases 1 to 4 respectively. For lower values of R_{sh} conduction block is observed.

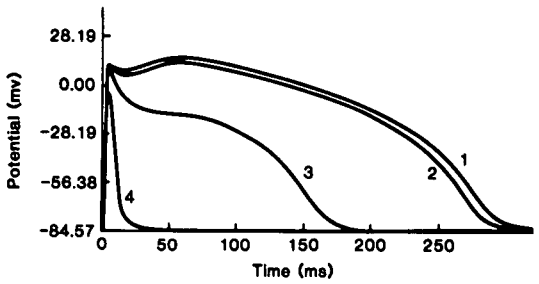

FIGURE 10. *Effects of variations in leakage resistance (R_{sh}) on the propagating action potential. Curves 1 to 4 correspond to progressively decreasing values of R_{sh} (see text).*

The effects of variations in R_{sh} on the ionic currents that constitute the Beeler and Reuter membrane model are shown in Figure 11. While the sodium current (I_{Na}) decreases by only about 10% in the range of R_{sh} considered, the slow currents (I_s, I_{x1}, and L_{k1}) that are associated with the plateau and repolarization phases are strongly affected and diminish in both amplitude and duration, bringing about the large change in the action potential duration.

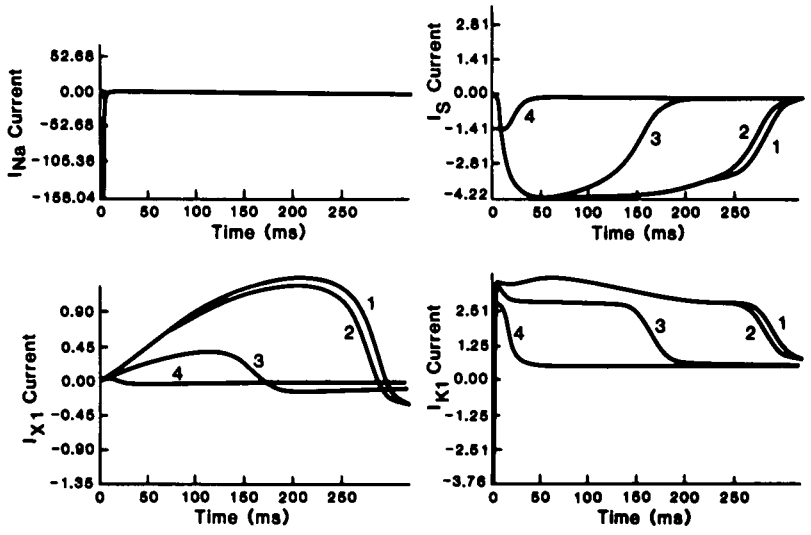

FIGURE 11. *Effects of variations in R_{sh} on the ionic currents that constitute the Beeler and Reuter model of the ventricular action potential. Curves 1 to 4 correspond to progressively decreasing values of R_{sh} as in Figure 10 above.*

Downloaded from http://ahajournals.org by on March 12, 2022

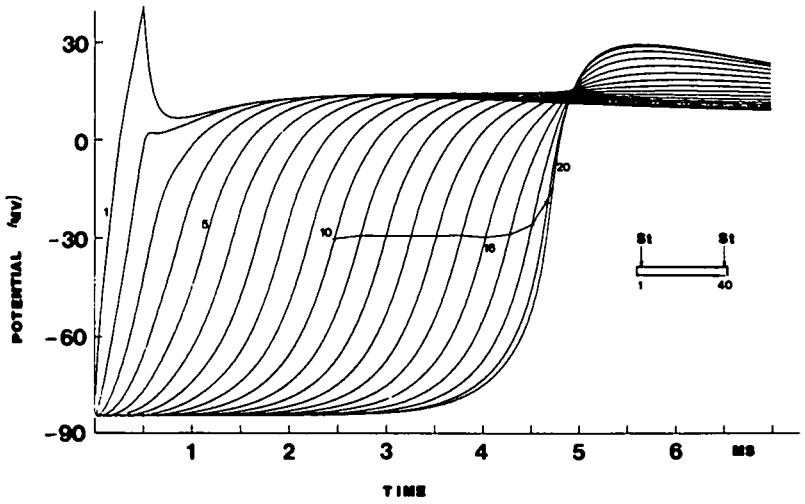

FIGURE 12. *The effects of collision on the propagating action potential. The fiber is stimulated simultaneously at both ends (see* inset*). The numbers in the body of the figure indicate the cell number in the fiber. The line connecting cells 10 through 20 marks the potential at which $\dot{V}_{max}$ is obtained. The collision site is at cell number 20.*

3. Collision

Because of the complex geometry of the myocardial structure, collisions of propagation wavefronts are likely to occur both at the cellular level and the global tissue level. In particular, the geometry and organization of the tissue suggests that multiple collisions can occur for propagation in a direction transverse to the fiber's orientation. The following simulation (Figure 12) examines the effects of collision at the cellular level in the one-dimensional discontinuous fiber. The model consists of 40 individual cells with symmetrical boundary conditions at both ends. Stimuli were applied simultaneously at both ends of the fiber, leading to a collision site at the 20th cell. The numbers in the body of the figure mark the cell number in the fiber. As the action potential approaches the collision site, several changes are observed. $\dot{V}_{max}$ increases progressively and is almost doubled at the collision site. In addition, $\dot{V}_{max}$ is obtained at progressively higher values of potential (marked by the line connecting the cells from 10 to 20 in the figure), and the amplitude (relative to the zero potential) increases as well. In contrast to the large increase in the value of $\dot{V}_{max}$, τ_{foot} shows a very small decrease of only 0.6%. The variations of these four variables ($\dot{V}_{max}$, the membrane potential V_m at $\dot{V}_{max}$, τ_{foot}, and the maximum potential amplitude V_m) as a function of distance from collision site are summarized in Figure 13.

4. Extracellular Potential

The rising phase of a spatial propagating action potential obtained from the discontinuous model is shown in Figure 14. Note the sharp discontinuities introduced at each intercalated disk location (arrows). In contrast, the action potential computed from a continuous model (no disks included) is smooth and does not exhibit sharp changes in slope (inset to Figure 14). The equivalent dipolar source density along the fiber is proportional to the slope of the action potential ($-\partial V_m/\partial X$ in equation 3). The source density is, therefore, very large at the disk. However, only a small fraction of the cell cross section is occupied by the connexons at the gap junction and is available for axial current flow. The effective cross section at the disk is only 0.01–0.03% of the total cross section based on morphological studies.[26] Taking this factor into account (equation 3a), the contribution to the extracellular field from sources at the disk becomes negligible as a result of the small cross-sectional area of the junctional region,[23] and the computed spatial extracellular poten-

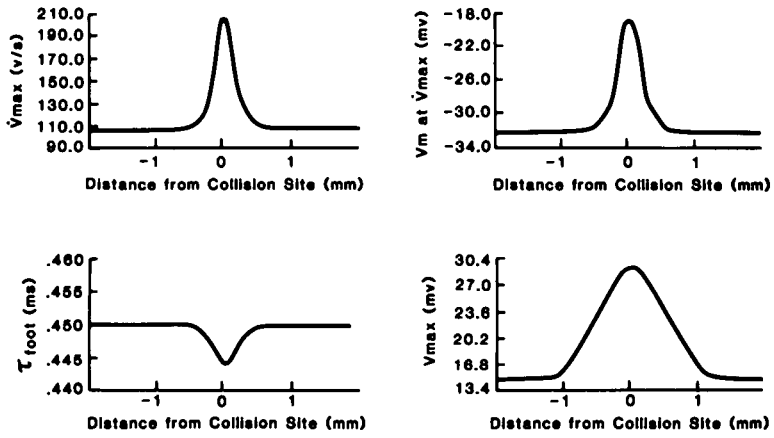

FIGURE 13. *A summary of the effects of collision (as a function of distance from the collision site) on $\dot{V}_{max}$; V_m (membrane potential) at which $\dot{V}_{max}$ is obtained; τ_{foot}; and V_{max} (maximum potential amplitude).*

Downloaded from http://ahajournals.org by on March 12, 2022

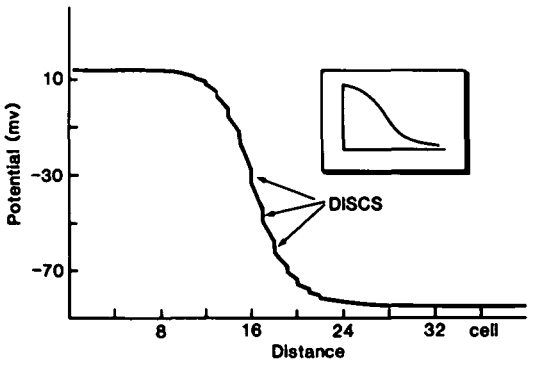

FIGURE 14. *Spatial action potential wavefront obtained from the discontinuous model. Note major discontinuities in leading edge at disk locations (arrows). A smooth action potential is shown for comparison* (inset).

tial at the surface of the fiber (Figure 15) is a smooth biphasic waveform that does not reflect the underlying discontinuous structure. This smoothing quality of the extracellular potentials and the fact that they do not reflect the discontinuities at a microscopic level were observed experimentally by Spach and Dolber.[7] In their measurements at sites 20–100 μm apart (less than a cell length), "the waveforms and their derivatives maintained a smooth contour, and there was a monotonic increase in the local activation times without evidence of local 'jumps' or 'delays'."

Discussion

The simulations described above demonstrate the importance of the structural discontinuities introduced by the intercalated disks in determining the characteristics of propagation in cardiac muscle. The propagation is discontinuous in nature with high velocity inside a cell and slower average (macroscopic) velocity over many cells. This discontinuous behavior becomes progressively more pronounced with increasing disk resistance. It should be emphasized, however, that over the normal physiologic range of disk resistance the discrete structure of the myocardium is not manifest in the behavior of the macroscopic velocity of propagation that follows closely the inverse square root relation of continuous cable theory. Only for high values of disk resistance (>20 $\Omega \cdot cm^2$) is deviation from this relation

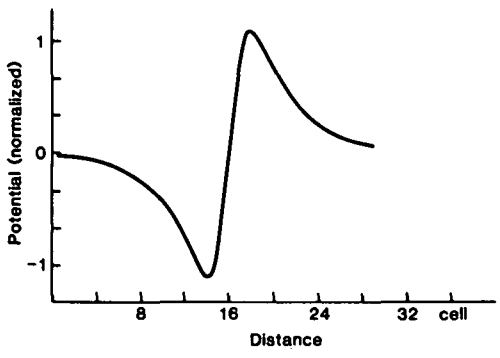

FIGURE 15. *Computed spatial extracellular potential at the surface of the discontinuous fiber.*

observed, and for very high disk resistance (>380 $\Omega \cdot cm^2$), decremental propagation and conduction block are obtained. In addition, the spatial extracellular potential along the fiber does not reflect the underlying discontinuities and resembles the smooth biphasic waveform of the continuous case.

In contrast to the above, several important characteristics of the propagating action potential are strongly influenced by the underlying discrete nature of the fiber. For a certain range of disk resistance a "paradoxical" increase in $\dot{V}_{max}$ with decreased velocity caused by higher disk resistance is observed. The behavior in this range can be explained on the basis of higher degree of confinement of the axial current flow to the activated cell. Under these conditions, the cell becomes increasingly separated from its downstream neighbor, more current is available at the site of depolarization, and $\dot{V}_{max}$ increases, approaching the value that could be obtained under space-clamp conditions (the nonpropagating "membrane action potential"). No significant change is observed in the magnitude of the fast inward current. Similar behavior (increased $\dot{V}_{max}$ with decreased velocity) was observed experimentally by Spach et al[2] for propagation transverse to the fiber axis. While Spach's results in a two-dimensional preparation can not be fully explained by a one-dimensional model, his experimental observations and our simulations consistently demonstrate the important role played by the tissue structure in determining the properties of propagation in cardiac muscle. It should be noted that for high values of disk resistivity (>70 $\Omega \cdot cm^2$) $\dot{V}_{max}$ starts to decrease (the descending limb in Figure 4) and a gradual transition to decremental propagation and eventually conduction block is observed. At this high degree of decoupling, the postjunctional charging current becomes increasingly limited, bringing about a decrease in the fast inward current. As a result, $\dot{V}_{max}$ decreases. Slow conduction with normal and low values of $\dot{V}_{max}$ is observed. For even higher values of disk resistance (>350 $\Omega \cdot cm^2$), the postjunctional current is too small to sustain propagation beyond several cells, and decremental conduction is observed (Figure 9). This complex nonmonotonic behavior of $\dot{V}_{max}$ implies that the common practice of using $\dot{V}_{max}$ as an index of conduction velocity is not valid for cardiac muscle when structural changes (decoupling) are involved. While conduction velocity is directly related to the square root of $\dot{V}_{max}$ when membrane properties alone are considered,[1,27,28] it is clear from our simulations (Figure 4) that in the discontinuous case $\dot{V}_{max}$ and conduction velocity are not related in a monotonic fashion when changes in disk resistance are introduced. Several studies of electrophysiologic changes in the border zone of myocardial infarcts during the healing and healed phases documented slow activation (conduction velocity of 0.03 m/sec) with normal action potentials (normal $\dot{V}_{max}$).[8,9,12] This observation is in accordance with the behavior of $\dot{V}_{max}$ seen in Figure 4. For a high disk resistance slow conduction with normal $\dot{V}_{max}$ is predicted by the model (the descending limb of the $\dot{V}_{max}$ curve). This simulation demonstrates that slow conduction, a necessary condition for reentrant ar-

Downloaded from http://ahajournals.org by on March 12, 2022

rhythmias, can be brought about by structural effects (decoupling) and is not necessarily a result of membrane changes in all cases.

Another important parameter is the foot of the action potential (τ_{foot}). In our simulations, τ_{foot} increases and conduction velocity decreases with increasing disk resistance. This result is in disagreement with the experimentally observed decrease in τ_{foot} for propagation transverse to the fibers in the actual multifiber preparation.[2] The complex geometry of cell connections and branching in the actual tissue suggests that many collisions may occur in this preparation. This motivated us to examine the effects of collisions in our discontinuous model. As a result of the collision, $\dot{V}_{max}$ is almost doubled. This result is consistent with the 80% increase in $\dot{V}_{max}$ observed by Spach et al.[2] A slight decrease in τ_{foot} is observed at the collision site in the simulation. The direction of this change is opposite to the increase in τ_{foot} caused by increased disk resistance; however, quantitatively the simulated effect is very small (only 0.6% change).

The simulations related to the effects of increased leakage current at the disk examine a situation that is not documented experimentally. However, it is possible that under abnormal conditions structural changes in the disk may occur that bring about a decrease in the leakage resistance. The major effect of an increase in the leakage current is to significantly shorten the duration of the propagating action potential (Figure 10). Such localized changes in regions of the myocardium can bring about nonuniformities in refractory periods and precipitate conditions of vulnerability to arrhythmias (reentry). In fact, short duration action potentials with very little evidence of a plateau phase were observed by Ursell et al[8] and by Kimura et al[12] in the border zone of experimental myocardial infarction. Kimura et al mention that "the mechanism underlying shortening of action potential duration in the border zone cells of the healed infarct preparations is unclear." They suggest a possible reduction in the slow inward current due to a decreased Ca^{2+} gradient at the plateau phase caused by an increase in intracellular Ca^{2+}. However, intracellular accumulation of Ca^{2+} is known to increase disk resistance and to cause cell-to-cell uncoupling and structural changes in the intercalated disk. These changes may bring about a decrease in the leakage resistance and result in a shortening of the action potential as predicted by the model.

References

1. Jack JJB, Noble D, Tsien RW: *Electric Current Flow in Excitable Cells*. Oxford, England, Clarendon Press, 1975
2. Spach MS, Miller WT III, Geselowitz DB, Barr RC, Kootsey JM, Johnson EA: The discontinuous nature of propagation in normal canine cardiac muscle. Evidence for recurrent discontinuities of intracellular resistance that affect the membrane currents. *Circ Res* 1981;48:39–54
3. Spach M, Kootsey JM, Sloan JD: Active modulation of electrical coupling between cardiac cells of the dog. A mechanism for transient and steady state variations in conduction velocity. *Circ Res* 1982;51:347–362
4. Plonsey R, Rudy Y: Electrocardiogram sources in a two dimensional anisotropic activation model. *Med Biol Eng Comput* 1980;18:87–95
5. Plonsey R, Barr RC: Current flow patterns in two-dimensional anisotropic bisyncytia with normal and extreme conductivities. *Biophys J* 1984;45:557–571
6. Barr RC, Plonsey R: Propagation of excitation in idealized anisotropic two-dimensional tissue. *Biophys J* 1984;45: 1191–1202
7. Spach MS, Dolber PC: Relating extracellular potentials and their derivatives to anisotropic propagation at a microscopic level in human cardiac muscle: Evidence for electrical uncoupling of side-to-side fiber connections with increasing age. *Circ Res* 1986;58:356–371
8. Ursell PC, Gardner PI, Albala A, Fenoglio JJ, Wit AL: Structural and electrophysiological changes in the epicardial border zone of canine myocardial infarcts during infarct healing. *Circ Res* 1985;56:436–452
9. Gardner PI, Ursell PC, Fenoglio JJ, Wit AL: Electrophysiologic and anatomic basis for fractionated electrograms recorded from healed myocardial infarcts. *Circulation* 1985;72: 596–611
10. Joyner RW: Effects of the discrete pattern of electrical coupling on propagation through an electrical syncitium. *Circ Res* 1982;50:192–200
11. Steinhaus BM, Spitzer KW: Simulation of activation sequence effects in heart tissue. *IEEE Frontiers of Engineering and Computing in Health Care*. Proceedings Fifth Conference IEEE EMBS 1983;5:199–204
12. Kimura S, Bassett AL, Gaide MS, Kozlovskis PL, Myerburg JL: Regional changes in intracellular potassium and sodium activity after healing of experimental myocardial infarction in cats. *Circ Res* 1986;58:202–208
13. Woodbury JW, Crill WE: On the problem of impulse conduction in the atrium, in Florey L (ed): *Nervous Inhibition*. New York, Plenum Press, 1961, pp 24–35
14. Page E, Shibata Y: Permeable junctions between cardiac cells. *Ann Rev Physiol* 1981;43:431–442
15. Freygang WH, Trautwein W: The structural implications of the linear electrical properties of cardiac Purkinje strands. *J Gen Physiol* 1970;55:524–547
16. Chapman JB, Fry CH: An analysis of the cable properties of frog ventricular myocardium. *J Physiol* (Lond) 1978;283: 263–282
17. Beeler GW, Reuter H: Reconstruction of the action potential of ventricular myocardial fibers. *J Physiol* (Lond) 1977; 286:177–210
18. Hodgkin AL, Rushton WHA: The electrical constants of a crustacean nerve fiber. *Proc R Soc Lond* 1946;133:444–508
19. Cooley JW, Dodge FA: Digital computer solutions for excitation and propagation in the nerve impulse. *Biophys J* 1966;6:583–599
20. Rush S, Larsen H: A particular algorithm for solving dynamic membrane equations. *IEEE Trans Biomed Eng* 1978;25: 389–392
21. Diaz PJ, Rudy Y, Plonsey R: Intercalated discs as a cause for discontinuous propagation in cardiac muscle: A theoretical simulation. *Ann Biomed Eng* 1983;11:177–189
22. Plonsey R: Action potential sources and their volume conductor fields. *Proc IEEE* 1977;65:601–611
23. Plonsey R, Barr RC: Effect of junctional resistance on source-strength in a linear cable. *Ann Biomed Eng* 1985;13:95–100
24. Tasaki I, Hagiwara S: Capacity of muscle fiber membrane. *Am J Physiol* 1957;188:423–429
25. Sasyniuk BI, Mendez C: A mechanism for re-entry in canine ventricular tissue. *Circ Res* 1971;28:3–15
26. Haas HG, Meyer R, Einwachter HM, Stuckem W: Intercellular coupling in frog heart muscle: Electrophysiological and morphological aspects. *Pflugers Arch* 1983;399:321–335
27. Hunter PJ, McNaughton PA, Noble D: Analytical models of propagation in excitable cells. *Prog Biophys Mol Biol* 1975; 30:99–144
28. Walton, MK, Fozzard HA: The conducted action potential: Models and comparison to experiments. *Biophys J* 1983; 44:9–26

KEY WORDS • discontinuous electrical propagation • discontinuous cable model • myocardial structure • intercalated disks • cell-to-cell conduction

Downloaded from http://ahajournals.org by on March 12, 2022